Jens Rüdiger Stellhorn, Shinya Hosokawa, and
Wolf-Christian Pilgrim*

# Microscopic Structure Analysis in Disordered Materials using Anomalous X-ray Scattering

**Abstract:** Although X-ray diffraction is still mainly used to determine crystal structures, the demand for an understanding of the atomic arrangement in disordered matter has progressively become more important over the past decades. However, apart from simple model systems, it is still a challenging task to unravel the microscopic ordering of the atoms in amorphous multi-component materials, although this knowledge becomes increasingly important in modern materials science, in which the physical properties are often related to the microscopic ordering of the different chemical species of the substance. This article reports about the combination of Anomalous X-ray Scattering (AXS) with Reverse Monte Carlo Computer simulation (RMC) as a proper tool to precisely determine the microscopic structural characteristics in such systems with high reliability. The basic principles of the method will be illustrated and some examples of modern materials will be given to proof the applicability and the capability of this method.

**Keywords:** Amorphous Materials, Glasses, X-ray Scattering, Anomalous Scattering, Microscopic Structure, Reverse Monte Carlo Simulation.

DOI 10.1515/zpch-2014-0555
Received June 26, 2014; accepted September 11, 2014

***Corresponding author: Wolf-Christian Pilgrim,** Department of Chemistry, Physical Chemistry, Philipps-University of Marburg, Hans-Meerwein-Strasse, 35032 Marburg, Germany, e-mail: pilgrim@staff.uni-marburg.de
**Jens Rüdiger Stellhorn:** Department of Chemistry, Physical Chemistry, Philipps-University of Marburg, Hans-Meerwein-Strasse, 35032 Marburg, Germany
**Shinya Hosokawa:** Department of Chemistry, Physical Chemistry, Philipps-University of Marburg, Hans-Meerwein-Strasse, 35032 Marburg, Germany; and Kumamoto University, Department of Physics, 2-39-1 Kurokami, Chuo-ku, Kumamoto 860-8555, Japan

# 1 Introduction

When X-rays are diffracted from crystals, they produce a characteristic pattern from which the periodic arrangement of the atoms in the crystalline material can be reconstructed. This observation was surely one of the groundbreaking discoveries of the early 20$^{th}$ century and has fundamentally influenced the advancement of physics and chemistry over the last one hundred years. It triggered the development of a completely new branch in experimental physics and chemistry and motivated the invention of numerous ingenious scattering techniques intended to image the microscopic structure and dynamics in condensed matter along a broad variety of length scales. The structural information obtained from countless diffraction experiments has since then strongly influenced our perception about the microscopic architecture of matter on the atomic level. The exceptional significance of scattering methods for the understanding of the microscopic properties in materials can also be inferred from the enormous efforts that are still being invested into the development of modern radiation sources to provide high brilliance radiation for increasingly sophisticated diffraction studies. The Institute Laue-Langevin and the ESRF in Grenoble/France or the ISIS-Spallation source in the UK and the FRM II reactor in Munich are just a few European examples. Other research centres are currently under construction and will be completed in the nearer future as e.g. the European free electron laser project XFEL in Hamburg and the European Spallation Source ESS which is going to be installed in Lund, Sweden.

In 1912, von Laue, Friedrich and Knipping asserted that X-rays are just electromagnetic oscillations with wavelengths in the range of about $10^{-9}$ cm. Von Laue was the first who concluded that such waves should be diffracted by the atomic Bravais lattices in ordinary crystals in the same way as is visible light by ordinary optical lattices [1]. To proof this statement he constructed a relative complex mathematical formalism which led to the formulation of the well known Laue equations. His conclusions were experimentally proofed shortly after by Friedrich and Knipping. Laue's equations define the interference conditions in three dimensional lattices and identify the exact relations between X-ray wavelength and the lattice parameters of the crystal.

Shortly afterwards, William Henry Bragg and his son William Lawrence made a similar discovery [2] while searching for a possibility to quantify the Bremsstrahlung spectra emitted from Cathode-tubes. However, their formulation – which is nowadays known as the famous Bragg-equation – appeared to be considerably simpler than von Laue's formalism since it directly related the distance $d$ between two coplanar lattice planes with the scattering angle $2\theta$ of an observed

diffraction peak if the X-ray wavelength $\lambda$ is known:

$$n \cdot \frac{\lambda}{2} = \mathrm{d} \cdot \sin(2\theta/2). \tag{1}$$

Although it can easily be shown that the Laue equations and the Bragg formula are essentially identical, the latter formulation is – presumably due to its simplicity – undoubtedly better known and regarded as the symbolic starting point for the vast development of scattering science in the subsequent decades.

Since von Laue's and Bragg's formalisms are only applicable to crystalline materials, the question immediately arose whether X-rays were also suitable to determine the arrangement of the atoms in disordered matter. It was therefore shortly after their discoveries, when Friedrich [3] and later Debye and Scherrer [4] extended their X-ray diffraction studies to liquids. They just observed few weak and diffuse rings on their photographic plates, which they interpreted as resulting from weaker molecular short range correlations and they concluded that liquids are not characteristic of long range ordering. In the following decade, other investigations on liquids followed and the fundamental theoretical relations to describe scattering pattern from statistically disordered materials appeared in 1927 by Zernike and Prins [5]. Nearly twenty years later a first review about scattering experiments on liquid samples was published by Gingrich [6]. Since then the number of structure explorations in liquids using X-rays and later neutrons did continuously increase. Two famous reviews were published in 1962 by Kruh [7] and by Furukuwa [8] summarizing the thitherto attained experimental and theoretical achievements in X-ray and neutron scattering on liquid systems.

In 1932 Zachariasen [9] published his famous paper about the atomic ordering in glasses where he concluded that the arrangement of the atoms in these solids must be fundamentally different from any crystalline ordering. He pointed out that glass structures may rather be described as chemically ordered random networks and that the spatial arrangement of the microscopic building blocks can fairly well be visualized as a frozen liquid. Shortly after, detailed X-ray scattering experiments on vitreous $SiO_2$ and $GeO_2$ were carried out by Warren [10] generally confirming this view. His results triggered a huge number of structure determinations on vitreous substances which still continues until today. Consequently, a number of articles appeared about the application of scattering techniques to glasses and the analysis of the corresponding scattering data (see e.g. [11]).

The determination of the microscopic structure in disordered materials is still a challenging task. Complex and complicated scattering techniques need to be applied and great efforts must be invested into data reduction and analysis before the scattering data can straightforwardly be interpreted. In the following, we will give a review on the contemporary use of anomalous X-ray scattering which in com-

bination with computer simulation methods has meanwhile become a powerful tool to determine the partial structural correlations in disordered multi component materials along a broad range of length scales. It allows investigating the relation between microscopic structure and physical properties in modern technically relevant materials, which make this method increasingly important.

## 2 Information content of the scattering intensities obtained from disordered materials

Diffraction studies on crystals and scattering experiments on amorphous materials differ in many aspects. E.g., in crystallography, it is common to represent the outcome of a diffraction experiment as a function of scattering angle $2\theta$. In scattering experiments on disordered materials, however, it is more opportune to use the so called scattering vector $\vec{Q}$ or its modulus instead. It is defined as the vector difference between the wave vectors of the scattered and the incident radiation $\vec{k}'$ and $\vec{k}_0$, respectively:

$$\vec{Q} = \vec{k}' - \vec{k}_0. \tag{2}$$

Since X-ray scattering can be regarded as being elastic, the moduli of the wave vectors are equal, i.e. $\left|\vec{k}'\right| = \left|\vec{k}_0\right| = 2\pi/\lambda$ and the modulus of $\vec{Q}$ amounts to

$$Q = 2k_0 \cdot \sin\left(\frac{2\theta}{2}\right), \tag{3}$$

in units on an inverse length. There also exists a substantial difference in the attainable scattering intensities: Bragg peaks, obtained from crystal diffraction are considerably more intense than is the scattering pattern obtained from disordered materials. This is due to the fact that if X-rays are deflected from crystal planes at a suitable scattering angle $2\theta$, where the scattering vector $\vec{Q}$ matches a reciprocal lattice vector, the diffraction condition is simultaneously fulfilled for a vast number of atoms with identical interatomic separation. Also, their real space correlation extends periodically along extremely wide ranges causing the signal width in reciprocal space, i.e. the Bragg peak, to narrow correspondingly. In a liquid or glass, the interatomic distances are continuously distributed and the diffraction condition is fulfilled at any angle. $\vec{Q}$ hence represents a continuous position vector in reciprocal space and it is more adequate to use this quantity as the scattering variable instead. Also, in disordered materials the correlation range in real space is usually short, not extending to about next or second next atomic neighbours. As a consequence the resulting diffraction peaks are widely broadened in reciprocal

space leading to weak scattering amplitudes. Therefore, the experimental intensity must be carefully corrected due to background contributions from container materials and other radiation sources as well as to intrinsic intensity contributions like Compton- or Fluorescence scattering. However, it must be mentioned at this point that exceptions exist concerning the short range nature of disordered materials: In network glasses the correlations can extend up to about 20 Å as was recently shown by Salmon and Zeidler [12].

The scattering amplitude is solely given by the superposition of all the waves emerging from the $N$ atomic scattering centres situated at their individual average positions. The intensity is then the square of the sum over all these waves weighted by their individual atomic form factors $f_n(\vec{Q})$ :

$$I(\vec{Q}) = \left| \left\langle \sum_{n=1}^{N} f_n(\vec{Q}) \cdot e^{-i\vec{Q}\cdot\vec{r}_n} \right\rangle \right|^2 = f(\vec{Q})^2 \left\langle \sum_{n,n'} \sum e^{i\vec{Q}\cdot(\vec{r}_n - \vec{r}_{n'})} \right\rangle . \tag{4}$$

$n$ and $n'$ in Equation (4) indicate the atomic positions and the angle brackets denote that the spatial situation of the $N$ atoms may be an ensemble averaged arrangement. To obtain the right hand side of Equation (4) it was assumed that all atoms in the sample are identical and contribute to the overall amplitude with the same form factor. Instead of Equation (4) we may then write

$$I(\vec{Q}) = N \cdot f(\vec{Q})^2 \cdot \frac{1}{N} \left\langle \sum_{n,n'} \sum e^{i\vec{Q}\cdot(\vec{r}_n - \vec{r}_{n'})} \right\rangle = N \cdot f(\vec{Q})^2 \cdot S(\vec{Q}), \tag{5}$$

which defines the structure factor characteristic of the explored sample:

$$S(\vec{Q}) = \frac{1}{N} \left\langle \sum_{n,n'} \sum e^{i\vec{Q}\cdot(\vec{r}_n - \vec{r}_{n'})} \right\rangle . \tag{6}$$

The structure factor $S(\vec{Q})$ is the central function to be obtained in scattering experiments on disordered materials. According to Equation (5) it can directly be obtained from the corrected scattering intensity $I(\vec{Q})$. If the sample consists of only one type of atoms, $S(\vec{Q})$ is a dimensionless quantity. It contains the total interference as a function of scattering vector and can hence be interpreted as a distribution function of interatomic pair distances in reciprocal space. In fact, it can be shown within the framework of statistical mechanics that $S(\vec{Q})$ is related to the *pair correlation function* $g(\vec{r})$ (see e.g. [13]) in real space. The values of this statistical function are proportional of finding an atom at position vector $\vec{r}$ when there is a reference atom located at the origin. $g(\vec{r})$ and $S(\vec{Q})$ are simply linked via a Fourier transformation:

$$g(\vec{r}) - 1 = \frac{1}{\rho_0 (2\pi)^3} \int \left( S(\vec{Q}) - 1 \right) e^{-i\vec{Q}\cdot\vec{r}} \, \mathrm{d}\vec{Q}, \tag{7}$$

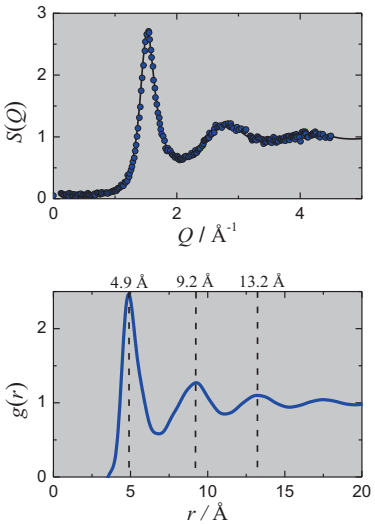


**Figure 1:** Structure factor and pair correlation function $g(r)$ as obtained from a neutron scattering experiment on liquid Rubidium close to melting [15].

where $\rho_0$ represents the particle density of the sample. Assuming complete structural isotropy, one may neglect the vector properties of $Q$ and $r$. Switching also to polar coordinates Equation (7) can be considerably simplified to give [14]:

$$g(r) - 1 = \frac{1}{2\pi^2 r\, \rho_0} \int_0^\infty Q \cdot [S(Q) - 1]\ \sin(Q\, r)\, \mathrm{d}Q, \tag{8}$$

which is much more useful for practical purposes. The pair correlation function $g(r)$ finally allows characterizing the explored disordered sample with respect to interatomic distances and coordination numbers. This is illustrated in Figure 1, where Structure Factor and Pair Correlation Function for liquid Rubidium close to its melting point are depicted as obtained from a neutron scattering experiment [15].

At sufficiently high density, i.e. close to melting, liquid alkali metals like Rb belong to the group of the so called simple liquids, i.e. they are monatomic disordered systems consisting of only one element where the atoms interact through radial symmetric forces. It can be seen from the Pair Correlation Function in Figure 1 that in liquid Rb a central atom is apparently surrounded by shells of next neighbours at distances of 4.9 Å, 9.2 Å and 13.2 Å as is indicated by the dashed vertical lines in the figure. The average number of particles in such shells can also be obtained from properly integrating the peaks of the corresponding radial dis-

tribution function $n(r) = 4\pi \cdot \rho_0 \cdot r^2 g(r)$. A value of 12 is obtained for the first shell of the present example indicating that an atom in liquid rubidium is on average surrounded by 12 next neighbours at a distance of 4.9 Å.

The identification of coordination numbers and interatomic distances is the purpose of basically any structure investigation on a disordered material. While this information characterizes simple monatomic systems like dense molten alkali metals unambiguously, this is no longer the case if the sample is more complex. The difficulties increase if the samples become chemically more realistic, i.e. if alloys or chemical mixtures of liquids and glasses are being explored. The procedure to deduce an expression for the scattering intensity of such samples is initially identical to the derivation of Equation (4), i.e. the pure scattering intensity is determined by the square of the sum of all waves emerging from the irradiated atoms. Primarily, the sum index may run over all atoms irrespective of their chemical nature. Depending on composition many different combinations of the scattering length factors appear then in the double sum preventing a factorization as in case of a simple monatomic system. As a consequence the structure factor of a mixture cannot be defined as a dimensionless quantity as in Equation (6) and it will retain the dimension of an area. Yet, all terms in the double sum have the same form and it appears more sensible to sum over the possible chemical combinations rather than over pairs of atom indices [16]. This approach leads to the following expression for the pure scattering intensity:

$$I(Q) = N\left(\left\langle f^2\right\rangle - \left\langle f\right\rangle^2\right) + N \cdot \left\langle f\right\rangle^2 S_{\mathrm{FZ}}(Q), \tag{9}$$

where the structure factor is now defined as

$$S_{\mathrm{FZ}}(Q) = \sum_{i,j}\sum w_{ij}(Q) \cdot S_{ij}(Q)$$
$$\text{with } w_{ij} = \frac{x_i x_j f_i f_j}{\left\langle f\right\rangle^2}. \tag{10}$$

It should be noted that the $Q$-dependence of the form factors $f(Q)$ in Equations (9) and (10) and in subsequent formulas has been omitted to preserve clarity.

$S_{\mathrm{FZ}}(Q)$ is the Faber–Ziman structure factor. $i$ and $j$ run over all combinations of chemical compositions, $f_i$ an $f_j$ are the respective form factors and $x_i$ and $x_j$ denote the corresponding molar fractions. The angle brackets now indicate averaging over the chemical composition. It should be noted that the structure factor in Equations (9) and (10) has subsequently been made dimensionless by normalizing it to the square of the average form factor in the sample. Rearranging Equation (9) finally gives a prescription how to extract the properly normalized

Faber–Ziman total structure factor from an experimental intensity $I(Q)$:

$$S_{\mathrm{FZ}}(Q) = \frac{\frac{C}{N} I(Q) - \left( \langle f^2 \rangle - \langle f \rangle^2 \right)}{\langle f \rangle^2}. \tag{11}$$

The constant $C$ has subsequently been introduced to ensure that the structure factor approaches unity for sufficiently large $Q$-values. $S_{\mathrm{FZ}}(Q)$ in Equation (11) is the experimentally accessible total structure factor of a multi-component system. According to Equation (10), it is composed of the partial structure factors $S_{ij}(Q)$. These quantities represent the correlation between particles of species $i$ to particles of species $j$ in reciprocal space. The partial structure factors are related to corresponding pair correlation functions $g_{ij}(r)$ in the same way as is $S(Q)$ to $g(r)$ in Equation (8):

$$g_{ij}(r) - 1 = \frac{1}{2\pi^2 r \rho_0} \int_0^\infty Q \cdot \left[ S_{ij}(Q) - 1 \right] \sin(Q r) \, \mathrm{d}Q. \tag{12}$$

The meaning of $g_{ij}(r)$ is similar to that of $g(r)$ for a pure sample. It determines the probability of finding a particle of species $j$ at position $r$ if there is another particle of species $i$ at the origin.

It should be mentioned that other definitions of partial structure factors exist in the literature. The Ashcroft-Langreth approach [17] is in principle similar to the Faber–Ziman method but defines scattering functions which oscillate around zero. However, it can be shown that both approaches are related [18]. Another commonly used formalism for binary mixtures is that of Bhatia and Thornton [19] where a set of partial structure factors is defined representing density-density, concentration-concentration and density-concentration correlations. It is also related to the Faber–Ziman approach as it can be shown that both can be expressed as a linear combination of the other if only two components are regarded [18]. An excellent survey is given in [20]. Throughout this article we will restrict ourselves to the Faber–Ziman formalism which appears to us to be more suitable for the physico-chemical questions addressed here.

Though $S_{\mathrm{FZ}}(Q)$ can directly be measured in an experiment, the relevant structural information is contained in the partial correlation functions. For a system consisting of $n$ components, $n(n+1)/2$ of these functions exist. Their determination is the ultimate goal in the structure exploration on a chemical mixture, but the partials are not directly accessible from conventional scattering experiments and specific efforts must be undertaken for their determination.

One possible approach to obtain the partial correlation functions for a multi-component system is to employ a Reverse Monte Carlo Simulation (RMC), where

the real sample is being simulated by a computer. In each simulation step the individual atoms are moved and the partial $g_{ij}(r)$ are calculated from the atomic positions in the computer generated ensemble. Using the inverse of the Fourier transform in Equation (12), the respective $S_{ij}(Q)$ can be computed to determine the total structure factor $S_{FZ}(Q)$ according to Equation (10). The simulation is then repeated until satisfactory agreement between the experimental and the computed total structure factors is reached. However, it should be kept in mind that this approach is just a fitting procedure with $n(n+1)/2$ free parameters and that their number is growing steeply with the number of chemical components. It is therefore appropriate to also include other boundary conditions into the simulation in order to make the result more unequivocally.

For a direct determination of the $n(n+1)/2$ unknown $S_{ij}(Q)$-functions of an $n$-component system an equally number of linear equations like Equation (10) were needed to form a linear set of inhomogeneous equations which can be solved numerically if the corresponding coefficient determinant is nonzero. Such additional equations, however, can only be generated if the $w_{ij}$- factors in Equation (10) can be modified without changing the chemical composition. Basically, this is possible in both X-ray- and neutron scattering. In the latter this can be achieved by preparing $n(n+1)$ different samples with differing isotopic composition of the sample components. In this case the form factors entering the weighting coefficients in Equation (10) have to be replaced by the average neutron scattering length of the isotopically manipulated sample constituents. In X-ray scattering, a variation of the form factors is also possible by a suitable energy variation of the incident radiation. The general procedure can be easily understood considering a gedankenexperiment on a model system consisting of just two different chemical components $A$ and $B$. According to Equation (10) the total structure factor is then given as

$$S_{FZ}(Q) = w_{AA}(Q) \cdot S_{AA}(Q) + 2 \cdot w_{AB}(Q) \cdot S_{AB}(Q) + w_{BB}(Q) \cdot S_{BB}(Q), \qquad (13)$$

where the coefficients are determined by the composition and the form factors in the sample:

$$w_{AA}(Q) = \frac{x_A^2 f_A^2}{\langle f \rangle^2}, \quad w_{BB}(Q) = \frac{x_B^2 f_B^2}{\langle f \rangle^2} \quad \text{and}$$
$$w_{AB}(Q) = \frac{x_A x_B f_A f_B}{\langle f \rangle^2}, \qquad (14)$$

with $x_i$ being the molar fraction of component $i$. The corresponding set of linear inhomogeneous equations then reads:

$$\begin{aligned} S^{I}_{\mathrm{FZ}}(Q) &= w^{I}_{AA} \cdot S_{AA}(Q) + 2 \cdot w^{I}_{AB} \cdot S_{AB}(Q) + w^{I}_{BB} \cdot S_{BB}(Q) \\ S^{II}_{\mathrm{FZ}}(Q) &= w^{II}_{AA} \cdot S_{AA}(Q) + 2 \cdot w^{II}_{AB} \cdot S_{AB}(Q) + w^{II}_{BB} \cdot S_{BB}(Q) \\ S^{III}_{\mathrm{FZ}}(Q) &= w^{III}_{AA} \cdot S_{AA}(Q) + 2 \cdot w^{III}_{AB} \cdot S_{AB}(Q) + w^{III}_{BB} \cdot S_{BB}(Q), \end{aligned} \tag{15}$$

where the $Q$-dependence of the weighting factors has again been omitted for clarity. The superscripts *I*, *II* and *III* stand for the different experiments where the coefficients are altered either by isotopic substitution or by an appropriate variation of the X-ray energy (note that for the neutron scattering case, the form factors always have to be replaced by the appropriate scattering lengths of the isotopic mixtures). In matrix notation Equation (15) reads:

$$\begin{pmatrix} S^{I}_{\mathrm{FZ}}(Q) \\ S^{II}_{\mathrm{FZ}}(Q) \\ S^{III}_{\mathrm{FZ}}(Q) \end{pmatrix} = \begin{pmatrix} w^{I}_{AA} & w^{I}_{AB} & w^{I}_{BB} \\ w^{II}_{AA} & w^{II}_{AB} & w^{II}_{BB} \\ w^{III}_{AA} & w^{III}_{AB} & w^{III}_{BB} \end{pmatrix} \cdot \begin{pmatrix} S_{AA}(Q) \\ 2S_{AB}(Q) \\ S_{BB}(Q) \end{pmatrix} \tag{16}$$

or

$$[S_{\mathrm{FZ}}] = [W] \cdot [S_{ij}].$$

Hence, the vector containing the partial structure factors is easily evaluated from knowing the experimentally determined vector of total structure factors and the matrix containing the weighting factors of Equation (15). The final accuracy of this method depends on one hand on the unavoidable experimental error but on the other hand also on the quality of the matrix $[W]$. It is preferable to chose the variation of the coefficients as to produce as much scattering contrast between the three experiments as possible, i.e. the resulting total structure factors should differ greatly. The value of the normalized determinant $|W|_n$ can be used as a measure for this quality [21] where normalization is achieved by dividing each row $r$ by $\sqrt{\sum_s w^2_{rs}}$, with $s$ indicating the column index. A modulus of $|W|_n = 1$ corresponds to the optimal case [21]. Poorly conditioned matrices lead to an unpredictable enhancement of the statistical error and may cause unphysical features in the resulting partial scattering functions.

As already mentioned, isotopic substitution in neutron scattering (NDIS) is the method of choice for this procedure. A large variety of successful NDIS-experiments were carried out in the past as e.g. the determination of the microscopic structural properties in vitreous $GeSe_2$ by Petri, Salmon and Fischer [22]. From the numerical evaluation of Equation (16) they obtained partial structure factors and corresponding pair correlation functions. The analysis of their data revealed detailed partial interatomic separations between the different sample constituents from which a clear picture of the relevant microscopic structures of this

material was obtained. This glass could be identified as consisting of a network of edge- and corner sharing $GeSe_4$-tetrahedra. Furthermore, the data analysis revealed the existence of homopolar Ge-Ge and Se-Se bonds. It was thitherto believed that such homopolar chemical correlations would not exist in vitreous systems, thus these structures are denoted as "wrong bonds".

Isotopic substitution in neutron scattering is a powerful technique for the determination of partial correlations in disordered materials. However, it is a difficult and highly sophisticated method which requires a lot of experience. Also, the substance under investigation must possess a variety of suitable and affordable isotopes causing sufficient contrast between the different $S_{FZ}(Q)$'s. Additionally, great care must be taken in order to determine the exact total structure factor for each sample and the statistical error should be as small as possible. Since different samples must be prepared, it must also carefully be ensured that the different isotopic compositions are really chemically identical. This is especially important for vitreous samples, since there the production process and the history of the sample can have a significant influence on the microscopic spatial properties.

As mentioned earlier, X-ray scattering also allows discriminating between different partial correlations in a mixture. A closer inspection of the interaction between the X-ray photon and the atom reveals that there exists an energy dependent contribution to the atomic form factor:

$$f(Q, E) = f_0(Q) + f'(E) + i\, f''(E). \tag{17}$$

$f_0(Q)$ in Equation (17) denotes the ordinary atomic form factor, which just represents the Fourier transform of the atomic electron density, while $f'(E)$ and $f''(E)$ are the real and imaginary parts of the complex energy dependent contribution. The imaginary part is characteristic of the absorption behaviour and the real part determines the dispersion which mainly influences the scattering strength of the element under consideration. These terms are usually small and can be neglected; however, they become significant when the incident energy is close to an absorption edge of the atom. This behaviour is denoted as the *anomalous dispersion*. It is illustrated in Figure 2 where the static atomic form factors for Ge and Se are exemplary shown in the upper diagram and the calculated energy dependent terms are depicted in the lower graph. The anomalous dispersion gave rise to the development of several techniques aiming to distinguish between the scattering from different atomic species in chemical mixtures and alloys [23–25]. It is tempting to make use of the anomalous dispersion in the same way as of the scattering length variation between different isotopes in NDIS: Measuring at $n(n + 1)/2$ different incident energies $E_k$, may then cause a contrast between the differently obtained total structure factors $S_{FZ}(Q, E_k)$ in an $n$-component mixture and a set of inhomogeneous linear equations similar as in Equation (15) may be formulated. The

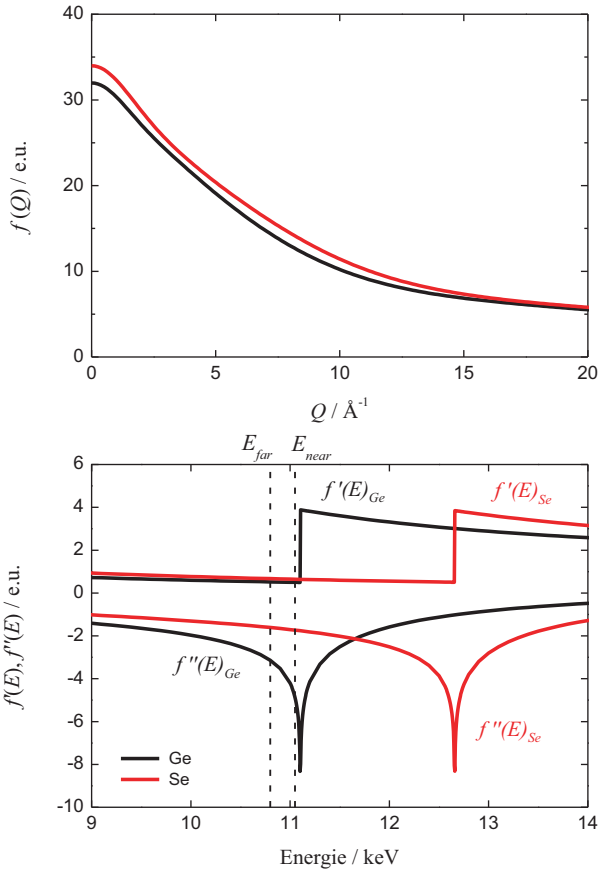


**Figure 2:** Static form factors for Ge (black line) and Se (red line) are shown in the upper graph. The lower graph gives the respective anomalous contribution. Both scales are given in electron units. As an example, $E_{\text{far}}$ and $E_{\text{near}}$ denote typical values used to determine differential scattering intensities at the Ge-*K*-edge (see text).

coefficients will then take the general form:

$$w_{ij}(Q, E_k) = \frac{x_i x_j \cdot f_i(Q, E_k) \cdot f_j^*(Q, E_k)}{\left|\langle f(Q, E_k)\rangle\right|^2}. \tag{18}$$

Here, $i$ and $j$ are again the indices of the chemical species. $f_i^*(Q, E_k)$ is the complex conjugate of the form factor in Equation (17). However, Figure 2 already indicates that the variation of the form factors with energy is only a few percent of the static $f_0(Q)$. This inevitably leads to a poorly conditioned coefficient matrix for the linear set of equations, i.e. the corresponding normalized determinant $|W|_n$

will always be much less than one. As already stated above, small errors in the measured $S_{FZ}(Q,E_k)$ will then cause capricious large errors in the partial structure factors. This problem cannot even be compensated if intense third generation synchrotrons like the ESRF in Grenoble are used as X-ray sources to improve the statistical quality of the data. Several attempts were undertaken in the past however, with only moderate success (see e.g. [26]) and therefore we will not further comment this approach here.

While one has only restricted influence on the statistical error of a measurement, it can be shown that systematic errors in the scattering data mainly cancel out if the method of differential intensities is employed [26]. Thereby, data measured at two different energies below an absorption edge of element $k$ are subtracted to give the differential structure factor $\Delta_k S(Q)$ of that specific element. The idea behind this approach is simple: Close to the edge, say about 20–30 eV below (see for example $E_{near}$ at the Ge-$K$-edge in Figure 2), the scattering from correlations of this component is weaker while correlations between the other elements in the sample scatter with normal intensity. Still farer below the edge, say about 200–300 eV, (see for example $E_{far}$ at the Ge-$K$-edge in Figure 2) scattering from the $k$-correlations is again increased. If the difference between the two measured intensities is taken, the scattering from the other correlations mainly drop out, since they are little affected by the energy variation and primarily correlations from the element under consideration will contribute to the differential scattering intensity. The differential structure factor $\Delta_k S(Q)$ can readily be obtained from the experimental intensities of Equation (9) taking into account an appropriate normalization [27]:

$$\Delta_k S(Q) \stackrel{\text{def}}{=} \frac{\Delta_k \left[C \cdot I(Q, E_{far}, E_{near})\right] - \Delta_k \left[\langle f^2 \rangle - \langle f \rangle^2\right]}{\Delta_k \left[\langle f \rangle^2\right]}. \tag{19}$$

$\Delta$ in Equation (19) denotes the difference of the subsequent quantity in square brackets taken between $E_{far}$ and $E_{near}$ close to the absorption edge of element $k$. This time normalization is achieved by dividing through the difference of the squared average form factors. This kind of normalization is on the one hand chosen as to retain the structure factor again dimensionless but also to obtain a reasonable scale for this quantity. Otherwise the values of the differential structure factor were extremely small along the entire $Q$-scale. Also, a constant $C$ is once again introduced to ensure that the structure factor approaches unity for sufficiently large $Q$-values. The experimental procedure is then repeated at the absorption edges of the other elements as well. As a result, one obtains the differential structure factors $\Delta_k S(Q)$ for each component $k$ of the mixture, each containing the correlations of this specific element to all elements in the sample. It is

in principle possible to Fourier transform these functions in order to get the corresponding differential pair correlation functions $\Delta_k g(r)$ which can then directly be interpreted (see e.g. [23, 26]). However, other possibilities exist allowing to draw more detailed structural conclusions from the data. The differential structure factors can also be related to the partial structure factors if Equation (13) is used to calculate $\Delta_k S(Q)$:

$$\Delta_k S(Q) = \sum_{i,j} \sum \Delta_k w_{ij}(Q) \cdot S_{ij}(Q). \tag{20}$$

According to Equation (18) and accounting for the normalization of Equation (19) the coefficients are then defined as

$$\Delta_k w_{ij}(Q, E_{\text{far}}, E_{\text{near}}) = \frac{x_i x_j \cdot \Delta[f_i \cdot f_j^*]}{\Delta[\langle f \rangle^2]}. \tag{21}$$

Again, the $\Delta$ indicate the differences of the quantities in the square brackets calculated at the different incident energies $E_{\text{far}}$ and $E_{\text{near}}$ at the edge of element $k$. For a two component system it is still possible to further pursue the approach of solving a set of inhomogeneous equations directly. For this a third measurement needs to be performed still further away from the aforementioned absorption edges of the sample elements. Then three measured structure factors exist and the set of inhomogeneous equations reads:

$$\begin{aligned} S(Q) &= w_{AA} \cdot S_{AA}(Q) + 2 \cdot w_{AB} \cdot S_{AB}(Q) + w_{BB} \cdot S_{BB}(Q) \\ \Delta_A S(Q) &= \Delta_A w_{AA} \cdot S_{AA}(Q) + 2 \cdot \Delta_A w_{AB} \cdot S_{AB}(Q) + \Delta_A w_{BB} \cdot S_{BB}(Q) \\ \Delta_B S(Q) &= \Delta_B w_{AA} \cdot S_{AA}(Q) + 2 \cdot \Delta_B w_{AB} \cdot S_{AB}(Q) + \Delta_B w_{BB} \cdot S_{BB}(Q). \end{aligned} \tag{22}$$

The first row in Equation (22) corresponds to the single $S(Q)$-measurement far away from the edges of the sample components, where the coefficients $w_{ij}(Q)$ are then calculated using Equation (18). The other two rows are determined by the differential structure factors at the $K$-edge of element $A$ and element $B$, respectively. Here, the coefficients are determined by Equation (21) (the $Q$-dependence of the coefficients in Equation (22) is again neglected for clarity). The advantage of solving Equation (22) instead of a set of equations obtained from directly measuring $S(Q,E_k)$ at three different energies is that the coefficient matrix of Equation (22) is considerably better conditioned. This is due to the fact that the differences in Equation (21) enhance those factors containing the form factors of the considered edge element and suppress the others. As a consequence, the experimental $\Delta_k S(Q)$'s comprise a considerably larger contrast than the directly measured $S(Q,E_k)$'s. The quality of the partial structure factors computed from this method is definitely improved as compared to results obtained from direct measurements

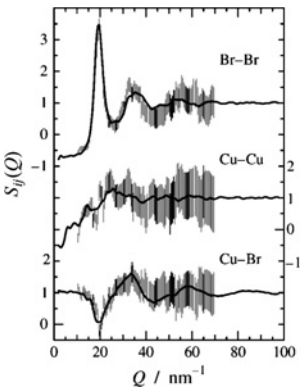


**Figure 3:** Partial structure factors of molten CuBr at 810 K (taken from ref. [28]). Vertical bars indicate the results obtained from numerically solving the linear equations of Equation (22). Solid lines correspond to values computed using a Reverse Monte Carlo simulation where a total $S(Q)$ and the corresponding $\Delta_k S(Q)$ are fed into the simulation.

at different energies; however, is still far from quantitative accuracy. This is illustrated in Figure 3 where some results obtained from this approach on molten CuBr are shown [28] as the vertical error bars. Still a considerable statistical fluctuation of the data is observed resulting from the unpredictable enlargement of the experimental statistical error by the still not perfectly conditioned coefficient matrix. I.e. the mathematically numerical peculiarities from solving inhomogeneous sets of equations still superimpose the physical content of the partial structure factors. However, there exists another alternative for the numerical solution making use of physically more reasonable arguments. This approach is based on the combination of the above mentioned Reverse Monte Carlo (RMC) technique with the differential structure factor method. Thereby, the experimental functions on the left hand side of Equation (22) are fed into the RMC-calculation. As already described above, the partial structure factors are then calculated in each step of the simulation using the atomic positions from the computer generated ensemble. The corresponding $S(Q)$ and $\Delta_k S(Q)$'s are then calculated using the respective weighting factors in Equation (22). The procedure is repeated until sufficient agreement is achieved between the experimental and the computed structure factors. In contrast to the simple RMC-analysis of a single total $S_{FZ}(Q)$ as described above, this procedure corresponds to the formal solution of a system with $n + 1$ linear equations and is therefore considerably more reliable. Of course the system of equations will always be under-determined for more than three components. Nevertheless, the advantage of this procedure as compared to the direct numerical evaluation of Equation (22) is that the obtained solutions are now based on

rather physical arguments, i.e. the movements of the respective atoms are determined by characteristic properties as e.g. the atomic diameters. Also, other physical and chemical constraints can be included into the simulation as e.g. molecular or mesoscopic structures known from other investigations or structural constraints due to electronic properties. Results from this procedure are also shown in Figure 3 as the solid lines. The overall agreement with the directly calculated values is clearly visible, but the data show considerably smaller errors.

Despite the apparent improvement of the structural information obtained from the AXS/RMC-combination, the resulting data still need to be critically scrutinized. It should always be kept in mind that the formal solution of an underdetermined system of linear equations can never lead to an unambiguous result. Therefore, the outcome of this procedure should be carefully tested as e.g. against other starting configurations. Also, as already mentioned above, it certainly improves the reliability of the data if other constraints are additionally included into the RMC-Simulation.

# 3 Experimental considerations

For the successful application of the AXS method as described above, some experimental aspects should be considered carefully, the main issues being the energy of the incident X-ray beam and the energy resolution of the experimental setup.

The choice of the incident energy is the crucial factor for the AXS method. For elements between the atomic numbers 23 and 52 (Vanadium to Tellurium), there usually exist experimentally accessible $K$ absorption edges. For elements heavier than Tellurium, $L$ absorption edges become experimentally more feasible, and also offer a contrast which is higher than that obtained at $K$ edges, as the variation of $f'(E)$ is more pronounced. Elements lighter than Vanadium, on the other hand, do not possess X-ray absorption edges in a suitable energy range. It should also be kept in mind that the choice of the incident energy defines the experimentally accessible $Q$-range, as the scattering angle is given by the experimental setup – in practice, this represents a problem especially for absorption edges below 10 keV, which would set a maximum $Q$-value of about 9 $\text{Å}^{-1}$ for a setup with $2\theta_{\max} \approx 120^{\circ}$. Furthermore, the two energies close to the edge needed for the calculation of the differential structure factor should be chosen as to provide properly enhanced weighting factors. But also here, the choice is limited by two factors (confer the exemplary schemes in Figure 2): on the near-edge side, values for the dispersion terms obtained from ab-initio calculations [29] can be employed, if the

**Table 1:** Weighting factors $w_{ij}(Q,E)$ and $\Delta_k w_{ij}(Q,E)$ for the total structure factor and for the differential measurements at each absorption edge in $Ge_2Sb_2Te_5$ for $Q = 20\,nm^{-1}$.

| Data | Ge-Ge | Ge-Sb | Ge-Te | Sb-Sb | Sb-Te | Te-Te |
|---|---|---|---|---|---|---|
| $S(Q)$ | 0.026 | 0.075 | 0.167 | 0.054 | 0.281 | 0.367 |
| $\Delta_{Ge}S(Q)$ | 0.125 | 0.243 | 0.608 | 0.002 | 0.01 | 0.012 |
| $\Delta_{Sb}S(Q)$ | 0.0001 | 0.136 | 0.028 | 0.191 | 0.545 | 0.100 |
| $\Delta_{Te}S(Q)$ | 0.0001 | −0.008 | 0.176 | −0.013 | 0.232 | 0.613 |

energy is chosen not too close to the edge (usually in the range of a few ten eV below the edge). Closer to the edge, electron correlation effects, which are neglected in these calculations, become important, so that the calculated values are not accurate enough anymore, and an individual measurement of the absorption edge by means of e.g. X-ray absorption spectroscopy becomes necessary (cf. [30]). On the far-edge side, the energy range is mainly limited by the variation of the dispersion terms of other constituent elements and by practical considerations due to the experimental setup. Consequently, this energy is usually chosen to be only a few hundred eV below the edge. This choice is by far one made most often, but it is not mandatory; an interesting example for an AXS experiment using energies very far from the absorption edge (i.e. 1.6 keV and 7 keV, respectively) can be found in [25, Chapter 5.1].

In Table 1, exemplary weighting factors for amorphous $Ge_2Sb_2Te_5$ are displayed for incident energies of 20 and 200 eV below the Ge-$K$-edge and of 30 and 300 eV below the other correspondent $K$ absorption edges, in contrast to the weighting factors of the total $S(Q)$ obtained for only a single measurement at 300 eV below the Te-$K$-edge. The enhancement of the contributions from the respective elements at their absorption edges is clearly visible. Note that the $w_{ij}$ are in principle $Q$-dependent, but change only on the scale of a few percent throughout the accessible $Q$-range.

Another important aspect is the energy resolution. While the necessary resolution of the incident beam is in the order of magnitude of a few eV (i.e. roughly $\Delta E/E = 10^{-4}$), is usually unproblematic to achieve at a modern synchrotron facility, the resolution of the detecting system – that is preferably in the range of 50 to 150 eV (i.e. about $\Delta E/E = 5 \times 10^{-3}$) – requires some explanation. The detector resolution needs to be sufficient in order to discriminate inelastic scattering contributions from the elastic signal; in the case of wide-angle anomalous scattering, these contributions are due to the Compton and the Resonant Raman effect (see e.g. [20] for further explanations on these effects), and can be sufficiently well determined with the specified resolution. On the other hand, a better resolu-

tion usually leads to a decrease of the measured intensity, and thus to a decrease in the statistical quality of the data, which is an essential factor for the calculation of the differential structure factors. Taking into account these considerations, the use of an analyzer crystal (e.g. graphite) and a standard scintillating detector have proven to be the best experimental compromise for this method. The use of a scintillating detector instead of e.g. a solid state detector greatly simplifies the data reduction procedure [31] and usually grants a higher counting rate. At the moment, this kind of experimental setup is only available at the beamlines BM02 at the ESRF and at BL13XU at SPring-8.

In the end, the concept of obtaining element specific information by use of the anomalous dispersion effect is of course not limited to the field of glassy structure determination or the differential AXS method. A contrast variation via the $f'(E)$ part of the form factor is also used in e.g. small angle scattering (ASAXS) [32]. On the other hand, the X-ray Absorption Fine Structure (XAFS) [33, 34] spectroscopy methods employ the structured imaginary part $f''(E)$ of the form factor above the absorption edge; and last but not least, a technique that employs the changes in both anomalous dispersion parts of the form factor is e.g. the Multi-wavelength Anomalous Diffraction (MAD) [35].

# 4 Examples

In the following part, we will show two selected examples for the application of the AXS-method coupled with RMC simulations used to investigate the structure of vitreous samples. We will discuss the merits of this method for determining partial correlations in multi-component systems by starting with a two-component system and then extend these considerations to three components.

The combination of AXS with RMC (AXS/RMC) was used in an extensive study to determine the concentration dependent structural properties of GeSe glasses [36]. Specific attention was attributed to the $GeSe_2$ composition [37], which allowed a direct comparison with the aforementioned NDIS data [22]. Results of this work are depicted in Figure 4(a) and (b). Symbols indicate experimental data from the AXS/RMC-method measured close to the Ge- and Se-$K$-edges. The $\Delta_k S(Q)$'s were obtained using Equation (19). Solid lines in Figure 4(a) represent the outcome from the RMC-simulation which is in very good agreement with the experimental data. The solid lines in Figure 4(b) are obtained from the NDIS-pair correlation functions [22] and corresponding X-ray weighting factors defined by Equation (21). Again, a good agreement is found and all features of the scatter-

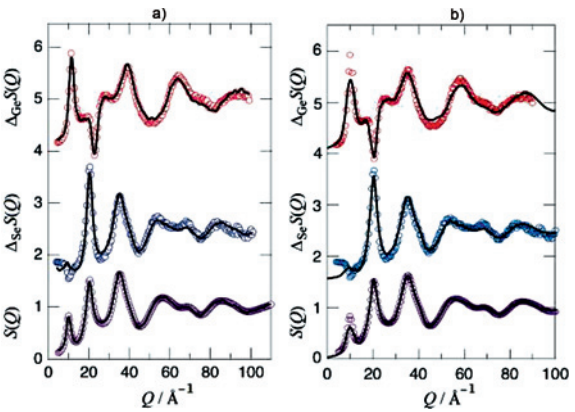


**Figure 4:** (a): Structure factor and differential structure factors of $GeSe_2$ obtained from AXS (symbols). Solid lines result from RMC-simulations where the total and the differential structure factors are calculated from the partials in each step using the weighting factors of Equations (18) and (21). The results are then compared with the experimental data. (b): Same experimental data as in (a) (symbols). Solid lines are calculated from the NDIS-partial pair correlation functions of [22] using the weighting factors defined in Equations (18) and (21).

ing functions are well resolved in both figures indicating the high reliability of the both methods.

The partial structure factors and pair correlation functions obtained from this AXS/RMC-approach are shown in Figure 5(a) and (b), respectively. They closely resemble the corresponding functions obtained from NDIS [22] which are also shown in the figure. All characteristic features seen in the NDIS-data are clearly resolved in the AXS/RMC-data as well. The AXS/RMC-approach also reveals that the so called prepeak, seen in the total structure factor at about 10 nm$^{-1}$, which is indicative for some kind of intermediate range ordering, does not only result from Ge-Ge correlations but also contains correlations between Ge and Se atoms. This is again in excellent agreement with the partials obtained in the aforementioned NDIS experiment [22]. Within the AXS/RMC-approach it is even possible to put this finding on a more quantitative basis. The data revealed that the fraction of Ge-Ge correlations contributing to this peak is only about 26% while the remaining intensity is due to Ge-Se correlations. Also, quantitative information on the abundance of Ge-Ge and Se-Se "wrong bonds" could be made and it was found that ten times more Se-Se bonds are present than corresponding Ge-bonds. Such quantitative information is possible since the method provides real space information obtained from the computer generated ensemble of the RMC-simulation.

Extending now the view from a two-component system, we will present another study on a glassy system with a ternary composition. Figure 6(a) shows to-

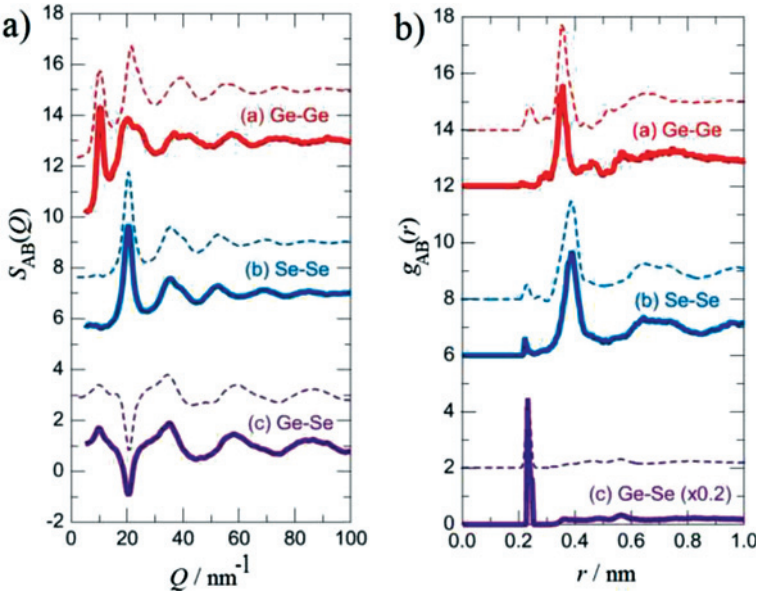


**Figure 5:** Partial structure factors (a) and partial pair correlation functions (b) of $GeSe_2$ obtained from the AXS/RMC-approach (see text). The pair correlation functions are in excellent agreement with the result obtained from NDIS [22] which are also shown as the dashed lines.

tal and differential structure factors obtained within the AXS/RMC-approach from the amorphous system $Ge_2Sb_2Te_5$ (GST) [38]. This substance is a so called Phase-Change Material and used for optical data storage on rewriteable compact disks as e.g. the Digital Versatile disc (DVD) or with a slightly different composition in the Blu-ray disc. Their functionality as rewriteable storage media is based on the ability to switch reversibly back and forth between a metastable crystalline and an amorphous phase, where this transition is accompanied by a substantial variation of the optical reflectivity. Also, the transition times are in the range of only some tens of nanoseconds allowing fast writing and erasing cycles. The origin for these remarkable properties is not yet understood, although these materials are used in industrial mass production for a long time. One reason for this lack of information is that the structural properties of the amorphous phases are still not comprehended. This is certainly due to the fact that the GST's are three-component systems and as mentioned above it is extremely difficult to reliably determine the six partial correlation functions needed to unambiguously characterise the structural correlations. No need to say that their direct determination as e.g. from NDIS-experiments is an extremely difficult if not even impossible task. Partial information about the atomic ordering in these systems could so far only be

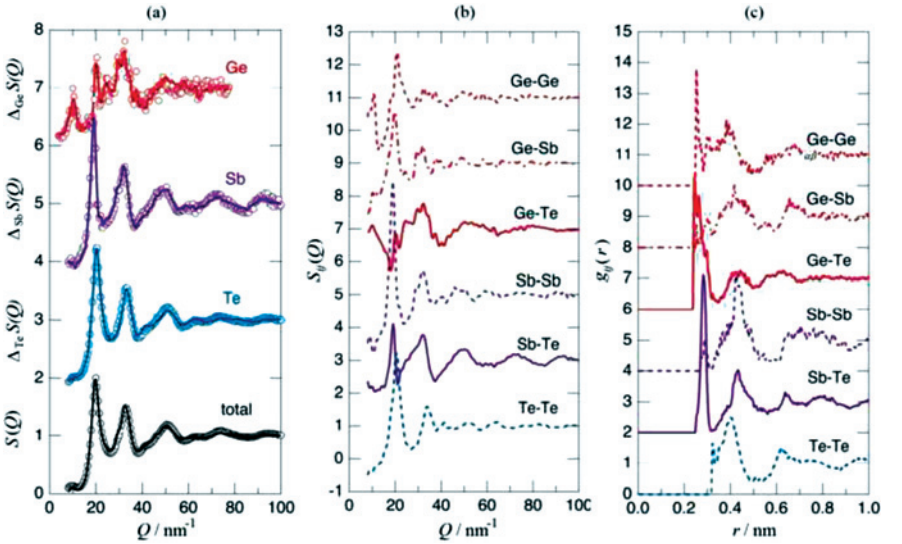


**Figure 6:** Results from the AXS/RMC-approach on $Ge_2Sb_2Te_5$. (a) shows the respective differential structure factors and the total $S(Q)$. Symbols represent the experimentally obtained data and the lines give the output of the RMC-analysis. Partial $S_{ij}(Q)$ and $g_{ij}(r)$ correlation functions as obtained from the RMC-simulation are shown in (b) and (c), respectively.

obtained from Extended X-ray Absorption Fine Structure (EXAFS) investigations. However, this method allows to access only the immediate vicinity around the examined atom. Partial correlations functions determined from the combination of RMC and EXAFS-data give therefore only an incomplete view of the real structural situation. This also hampers the accuracy of coordination numbers obtained exclusively from EXAFS-investigations in disordered systems [39].

Hence, the AXS/RMC-approach appears to be ideally suited to investigate these ternary systems. The experimentally obtained differential and total structure factors presented in Figure 6(a) show a very good overall agreement with the RMC-simulated functions given as the solid lines. The partial structure factors and pair correlation functions obtained from the computer generated ensemble are shown in Figure 6(b) and (c), respectively. The results gave some interesting new insight into the structural properties of this material, which could hitherto only be investigated using RMC-calculations on total structure factors [40] or from different types of ab initio computer approaches [39–41].

The measured structure factors in Figure 6(a) are already quite informative: A small prepeak is observed at about 10 $nm^{-1}$ in $S(Q)$ indicating the existence of intermediate range correlations. A comparably strong peak is however only visible in $\Delta_{Ge}S(Q)$ indicating that this feature originates mainly from correlations

related to the Ge atom (for the respective partial pair contributions to the differential structure confer also Table 1). Also, $\Delta_{Te}S(Q)$, $\Delta_{Sb}S(Q)$ and $S(Q)$ resemble each other while the $\Delta_{Ge}S(Q)$ is quite different. While the former structure factors comprise a strong main maximum at about 20 $nm^{-1}$ this is not visible in the Ge-related function. This clearly indicates that the local and intermediate ordering around the Ge-atom in the glass must be considerably different from the microscopic spatial ordering of the other elements.

The partial $S_{TeTe}(Q)$ and $S_{SbSb}(Q)$ in Figure 6(b) are quite similar indicating again a comparable local environment around these two atoms. This is also comparable to the structural situation in the related metastable crystalline phase which has a rocksalt-like structure where the Te-atoms constitute one of the two interpenetrating cubic lattices while the Sb- and Ge-atoms make up the other. In fact, the corresponding Sb-Te-pair correlation in Figure 6(c) shows a strong and sharp peak at about 0.28 nm nearly corresponding to the same distance in the crystal. This observation suggests that some structural features from the crystal may survive the transition into the amorphous phase. As already concluded from the experimental scattering laws, the Ge-atoms seem to behave structurally different from the other constituents. This is also seen in the related partials pair correlations which considerably deviate from the other functions. Strong direct correlations between Ge-Te and Ge-Ge are found. The latter is again a so called "wrong" bond. No indications for such bonds are observed for Te and only to a small extent for Sb. The Ge-Ge bond seems even to be a prominent feature in the amorphous phase of $Ge_2Sb_2Te_5$ which is considerably different to the crystalline phase.

More quantitative structural information can be obtained from directly inspecting the real space arrangement of the atoms in the computer generated RMC-ensemble. A section of this ensemble is depicted in Figure 7(a). It allows direct identification of the structural origins of many of the features seen in the correlations functions of Figure 6. Figure 7(a) reveals tetrahedral and pyramidal units around the Ge- and Sb-atoms, which are separately depicted in Figure 7(b) and (c). Also, $Sb–Te_3$ pyramidal units together with a small portion of T-shaped units are found both can be interpreted as fragments of the original Te-Sb rock salt crystal structure. Figure 7(d) shows square ring units extracted from Figure 7(a). They preferably consist of $Ge_2Te_2$-units. Square rings structures were already predicted in several ab initio calculations [42, 43] where they were interpreted as characteristic fragments of the related crystal structure and it was speculated that these structural units may be responsible for the fast crystalline-amorphous transition. The AXS/RMC-result is generally in accord with this hypothesis; however, the data also reveal that these units are not simply flat square rings as was believed so far, but that they are folded along the Te-Te axis. This is an important observation supportive to also understand the variation of the optical properties dur-

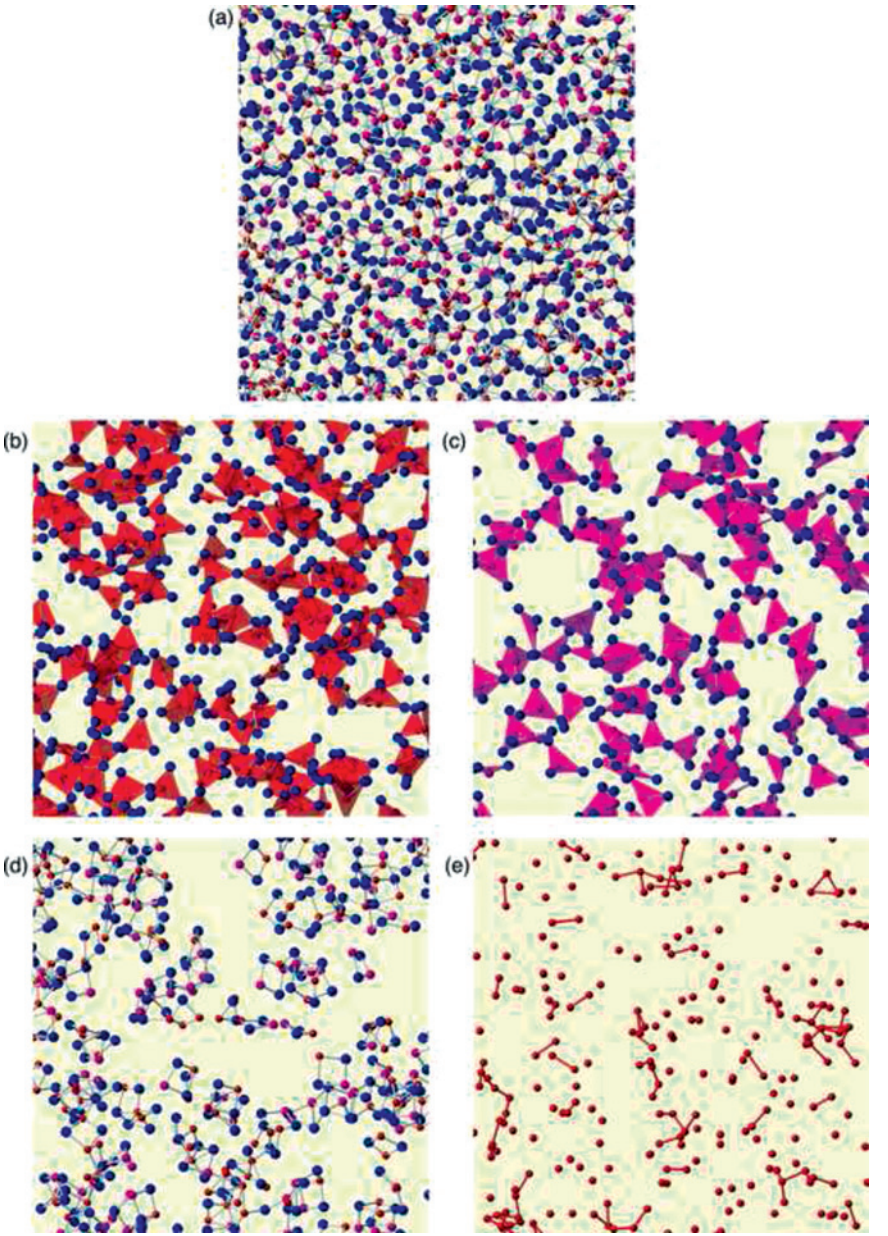


**Figure 7:** (a) An example of atomic configuration of Ge (red), Sb (purple), and Te (blue) atoms. (b) Tetrahedral or pyramidal units around the Ge atoms. (c) Those around the Sb atoms. (d) Square rings made of mainly Ge–Te–Ge–Te with puckered shapes. (e) The Ge atoms with the wrong bonds given by bars.

ing the crystalline-amorphous transition in these systems (for more information see [44]). The observation of folded rings is also in agreement with results from direct investigations of the $Ge_2Te_2$ aggregates in molecular beam experiments [45]. It should be mentioned that about 40% of the Ge- and Te-atoms belong to such ring structures in this GST-material.

Figure 7(e) shows the spatial arrangement of the Ge atoms extracted from Figure 7(a). The existing "wrong" Ge–Ge bonds are represented by bars. Interestingly, a quite large number of Ge-chains is observed. Their existence cannot be explained by a simple mechanism taking into account fragments from the original crystal structure and other mechanisms must be considered to explain these structural units. The remarkable physical properties of the GST-phase change materials have led to a number of structural speculations in order to explain transition mechanisms and the variation in the optical properties. The AXS/RMC-approach has considerably contributed to unravel at least some of the related questions and could even put some of the assumptions on a more quantitative basis. It is to be expected that the systematic investigation of phase change GST's with different composition may lead to even more knowledge about the role of specific constituents in these systems.

These two examples of multi-component systems show that, beside the high quality of the obtained partial correlation functions and the possibility to directly identify real space spatial atomic arrangements in the computer generated ensembles there exists another important advantage of the AXS/RMC-method: In the direct approach where $n(n + 1)/2$ inhomogeneous linear equations of an $n$-component system must be solved, the same number of experiments is required. Since the number of equations rises steeply with increasing number of constituents, the direct method becomes increasingly unfeasible from the technical and also from the monetary point of view. E.g., for a three component system, six equations must be solved and as much different isotopic compositions were needed in the NDIS-approach. The AXS/RMC-approach, however, still allows a quite reliable investigation of such systems although the resulting set of equations becomes inevitably under-determined. In a three component system instead of the six required functions, only three differential structure factors and one total $S(Q)$ are accessible. However, they are fed into the RMC-simulation where these coupled equations are solved simultaneously on the basis of physical arguments. Therefore, the corresponding results retain a very high degree of reliability. This approach is at current the best one can do to investigate multi-component disordered systems and the obtained partial correlations are in any case more trustworthy than those obtained from the direct RMC-analysis of simple total $S(Q)$-data.

# 5 Conclusions

In the present article we have closely illustrated one of the many modern techniques that have been developed for the characterization of materials since the first discoveries of Max von Laue and William Henry and William Lawrence Bragg in the early 20$^{th}$ century. We have thereby described how the diffraction of X-rays in general can not only be used to study crystalline matter, but also to investigate how disordered materials produce characteristic scattering patterns and how structural information can be obtained from the measured data. We have demonstrated that structural information like partial coordination numbers and atomic distances can be determined even in chemically complicated systems by utilizing the anomalous dispersion effect, and that the additional use of computer simulation techniques can be of great benefit for the interpretation of the resulting scattering functions. Such data are nowadays extremely important for material science to understand chemical, mechanical and optical properties of modern technically relevant materials.

The determination of structural properties in disordered substances is still one of the most active research fields within the scattering communities and a lot of effort is still invested to develop new scattering techniques and methods and to establish new and high-performance radiation sources for such investigations. While the motivation for this research field was originally motivated by pure fundamental research, it has nowadays turned into an important research branch for applied science which allows to directly link the physical properties of disordered materials to characteristic structural features on the atomic and mesoscopic level.

**Acknowledgement:** The authors would like to thank the contacts and local staff at the ESRF in Grenoble, France, and acknowledge the great experimenting conditions at this facility.

# References

1. M. Laue, W. Friedrich, and P. Knipping, Münchener Sitzungsberichte (1912) 303, imprinted in W. Friedrich, P. Knipping, and M. Laue, Ann. Phys. **41** (1913) 971. M. Laue, Ann. Phys. **41** (1913) 989.
2. W. H. Bragg, and W. L. Bragg, Proc. Roy. Soc., Ser. A **88** (1913) 428. W. H. Bragg, and W. L. Bragg, Proc. Roy. Soc., Ser. A **89** (1913) 246. W. H. Bragg and W. L. Bragg, Proc. Roy. Soc., Ser. A **89** (1913) 248. W. L. Bragg, Z. Phys. Chem. **104** (1915) 337.
3. W. Friedrich, Phys. Z. **14** (1913) 317.

4. P. Debye and P. Scherrer, Nach. Gött. Ges. (1916) 16.
5. F. Zernike and J. A. Prins, Z. Phys. **41** (1927) 184.
6. N. S. Gingrich, Rev. Mod. Phys. **15** (1943) 90.
7. R. F. Kruh, Chem. Rev. **62** (1962) 319.
8. K. Furukawa, Rep. Prog. Phys. **25** (1962) 395.
9. W. H. Zachariasen, J. Am. Chem. Soc. **54** (1932) 3841.
10. B. E. Warren, Phys. Rev. **45** (1934) 657.
11. A. C. Wright, in: *Neutron and Synchrotron Radiation for Condensed Matter Studies, Applications to Solid State Physics and Chemistry*, Chapter 8, J. Baruchel, J. L. Hodeau, M. S. Lehman, J. R. Regnard, C. Schlenker (Eds.), Springer-Verlag, Berlin, Heidelberg (1994).
A. C. Wright, The Structure of Amorphous Solids by X-ray and Neutron Diffraction, in: *Advances in Structure Research by Diffraction Methods*, Volume 5, W. Hoppe, R. Mason (Eds.), Pergamon, Oxford (1974).
12. P. S. Salmon and A. Zeidler, Phys. Chem. Chem. Phys. **15** (2013) 15286.
13. F. Kohler, *The Liquid State*, Verlag Chemie, Weinheim (1972).
P. Egelstaff, *An Introduction to the Liquid State*, 2nd Edn., Clarendon Press, Oxford (1994).
J. S. Higgins and H. C. Benoit, *Polymers and Neutron Scattering*, Clarendon Press, Oxford (1996).
14. P. Debye, Ann. Phys. **46** (1915) 809.
15. G. Franz, W. Freyland, W. Gläser, F. Hensel, and E. Schneider, J. de Physique Coll. **41** (1980) 194.
16. T. E. Faber and J. M. Ziman, Phil. Mag. **11** (1965) 153.
17. N. Ashcroft and D. C. Langreth, Phys. Rev. **156** (1967) 685.
18. N. E. Cusack, *The Physics of Structurally Disordered Matter*, Hilger, Bristol (1987).
19. A. B. Bhatia and D. E. Thornton, Phys. Rev. B **2** (1970) 3004.
20. H. E. Fischer, A. C. Barnes, and P. S. Salmon, Rep. Prog. Phys. **69** (2006) 233.
21. F. G. Edwards, J. E. Enderby, R. A. Howe, and D. I. Page, J. Phys. C: Solid State Phys. **8** (1975) 3483.
22. I. Petri, P. S. Salmon, and H. E. Fischer, Phys. Rev. Lett. **84** (2000) 2413.
P. S. Salmon and I. Petri, J. Phys.: Condens. Matter **15** (2003) 1509.
23. P. H. Fuoss, P. Eisenberger, W. K. Warburton, and A. Bienenstock, Phys. Rev. Lett. **46** (1981) 1537.
24. Y. Waseda, *The Structure of Non-Crystalline Materials*, McGraw-Hill, New York (1980).
25. Y. Waseda, *Anomalous X-ray Scattering for Materials Characterization, Springer Tracts in Modern Physics*, Vol. 179, Spinger-Verlag, Berlin, Heidelberg (2002).
26. K. F. Ludwig, W. K. Warburton, L. Wilson, and A. I. Bienenstock, J. Chem. Phys. **87** (1987) 604.
27. W.-C. Pilgrim, J. R. Stellhorn, and S. Hosokawa, Bunsen. Mag. **15** (2013) 131.
28. Y. Waseda, S. Kang, K. Sugiyama, M. Kimura, and M. Saito, J. Phys.: Condens. Matter **12** (2000) A195.
29. D. T. Cromer and D. Liberman, J. Chem. Phys. **53** (1970) 1891.
30. L. Kissel, B. Zhou, S. C. Roy, S. K. Sen Gupta, and R. H. Pratt, Acta Cryst. A **51** (1995) 271.
31. S. Hosokawa, W.-C. Pilgrim, J.-F. Bérar, and S. Kohara, Eur. Phys. J. Special Topics **208** (2012) 291.
32. G. Goerigk, H.-G. Haubold, O. Lyon, and J.-P. Simon, J. Appl. Cryst. **36** (2003) 425.
33. B.-K. Teo, *EXAFS: Basic Principles and Data Analysis*, Springer, Berlin, Heidelberg, New York, Tokyo (1986).

34. J. J. Rehr, R. C. Albers, Rev. Mod. Phys. **72** (2000), 621.
35. W. A. Hendrickson, Science **254** (1991) 51.
36. S. Hosokawa, Y. Wang, J.-F. Berar, J. Greif, W.-C. Pilgrim, and K. Murase, Z. Phys. Chem. **216** (2002) 1219.
37. S. Hosokawa, W.-C. Pilgrim, J.-F. Bérar, and S. Kohara, Phys. Status Solidi A **208** (2011) 2544.
38. S. Hosokawa, W.-C. Pilgrim, A. Höhle, D. Szubrin, N. Boudet, J.-F. Berar, and K. Maruyama, J. App. Phys. **111** (2012) 083517.
39. P. Jóvári et al., J. Phys: Conden. Matter **19** (2007) 335212.
40. S. Kohara, K. Kato, S. Kimura, H. Tanaka, T. Usuki, K. Suzuya, H. Tanaka, Y. Moritomo, T. Matsunaga, N. Yamada, Y. Tanaka, H. Suematsu, and M. Takata, Appl. Phys. Lett. **89** (2006) 201910.
41. S. Caravatti, M. Bernasconi, T. D. Kühne, M. Krack, and M. Parinello, Appl. Phys. Lett. **91** (2007) 171906.
42. J. Akola and R. O. Jones, Phys. Rev. B **76** (2007) 235201.
43. J. Hegedüs and S. R. Elliott, Nat. Mater. **7** (2008) 399.
44. B. Huang and J. Robertson, Phys. Rev. B **81** (2010) 081204.
45. R. Schäfer, S. Schlecht, J. Woenckhaus, and J. A. Becker, Phys. Rev. Lett. **76** (1996) 471.